Inorganic Chemistry

Article

pubs.acs.org/IC

Rapid Microwave-Assisted Solvothermal Synthesis of Non-Olivine *Cmcm* Polymorphs of $LiMPO_4$ (M = Mn, Fe, Co, and Ni) at Low Temperature and Pressure

Gaurav Assat and Arumugam Manthiram*

Department of Mechanical Engineering, The University of Texas at Austin, Austin, Texas 78712, United States

Supporting Information

ABSTRACT: Lithium transition-metal phosphates, $LiMPO_4$ (M = Mn, Fe, Co, and Ni), have attracted significant research interest over the past two decades as an important class of lithium ion battery cathode materials. However, almost all of the investigations thus far have focused on the olivine polymorph that exists in the orthorhombic *Pnma* space group. In this study, a distinct orthorhombic but non-olivine polymorph of $LiMPO_4$, described by a *Cmcm* space group symmetry, has been synthesized with M = Mn, Fe, Co, and Ni. Of these, $LiMnPO_4$ in the *Cmcm* space group is reported for the first time. A rapid microwave-assisted solvothermal (MW-ST) heating process with tetraethylene glycol (TEG) as the solvent and transition-metal oxalates as precursors facilitates the synthesis of these materials. The peak reaction temperatures and pressures were below 300 °C and 30 bar, respectively, which are several orders of magnitude lower than those of the previously reported high-pressure (gigapascals) method. X-ray diffraction (XRD) confirms the crystal structure with the *Cmcm* space group, and scanning electron micrographs indicate a submicrometer thin platelet-like morphology. The synthesis process conditions have been optimized to obtain impurity-free samples with the correct stoichiometry, as characterized by XRD and inductively coupled plasma-optical emission spectroscopy (ICP-OES). Upon heat treatment to higher temperatures, an irreversible transformation of the metastable *Cmcm* polymorphs into olivine is observed by XRD and Fourier transform infrared spectroscopy. Although the electrochemical activity of these polymorphs as lithium ion cathodes turns out to be poor, the facile synthesis under mild conditions has permitted easy access to these materials in a nanomorphology, some of which were not even possible before.

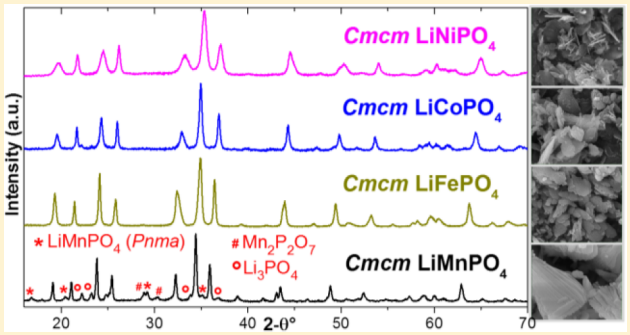

INTRODUCTION

For the advancement of lithium ion batteries, polyanion cathode materials[1] have attracted a significant amount of research attention starting with the early investigations of $Fe_2(SO_4)_3$ and $Fe_2(MO_4)_3$ (M = Mo and W) in the 1980s.[2,3] Most notably, the discovery of $LiFePO_4$ in the 1990s as a viable lithium ion cathode material[4] brought the entire class of $LiMPO_4$ (M = Mn, Fe, Co, and Ni) compounds into the spotlight, and several papers about these have been published over the past two decades.[5−8] These lithium transition-metal phosphates are more commonly termed phospho-olivine cathode materials because of their orthorhombic crystal structure with *Pnma* space group symmetry. Numerous strategies have been examined to optimize the performance of these cathodes, including but not limited to nanosizing,[9] conductive carbon coating,[10] conductive polymer coating,[11] making solid solutions,[12,13] and cation doping.[14] However, almost all the investigations have been performed with the olivine structured base materials, leaving only a handful of reports about $LiMPO_4$ polymorphs having a different kind of crystal structure.

For the first time, in 2001, polymorphs of $LiFePO_4$ and $LiNiPO_4$, represented by the orthorhombic *Cmcm* space group, were reported but exhibited no electrochemical activity.[15] These were obtained as a result of phase transition of the corresponding olivine materials upon the application of significantly high pressure (65 kbar) and high temperature (1173 K). Later, in 2009, the same high-pressure method was extended to obtain the *Cmcm* polymorph of $LiCoPO_4$, but the electrochemistry was not studied.[16] The high-pressure method could not be successfully applied for the synthesis of *Cmcm* structured $LiMnPO_4$. Some papers call this structure "*β*" phase, "Na_2CrO_4 like", or "$CrVO_4$ like" phase, while the olivine structure has been called the "*α*" phase. To avoid confusion, this report will use the space group symbols, *Cmcm* and *Pnma*, for the non-olivine and olivine polymorphs, respectively.

In a 2010 report, the *Cmcm* polymorph of $LiNiPO_4$ was partially obtained with a phosphate-formate precursor heated at 500 °C with only a 44% phase purity, the remaining 56% being olivine.[17] In 2012, a low-temperature (150 °C), water-free liquid-phase method was developed for the precipitation of *Cmcm* $LiFePO_4$ as a pure phase.[18] Even though these two

Received: August 5, 2015
Published: October 2, 2015

DOI: 10.1021/acs.inorgchem.5b01787
Inorg. Chem. 2015, 54, 10015−10022

methods circumvented the application of high pressure, they could not be applied for the other $LiMPO_4$ analogues.

Microwave-assisted heating of liquid-phase reaction media is being employed increasingly as a synthesis method for inorganic nanostructures.[19−21] The distinctive characteristics of microwave-assisted syntheses are fast heating rate, low reaction temperature, low pressure, very short reaction duration, and superior repeatability. As a result, this kinetically driven reaction opens up the possibility of obtaining low-temperature metastable phases and polymorphs, which could not be synthesized with conventional techniques.[14,22,23] A microwave-assisted synthesis of *Cmcm* $LiFePO_4$ was reported in 2013 with absolutely dry precursors (prepared in an argon-filled glovebox) in a 1:1 solvent mixture of benzyl alcohol and 2-pyrrolidinone as the reaction medium.[24] It was also shown that the solvent ratio played an important role in deciding which polymorph formed primarily. In 2014, a different microwave-assisted synthesis reported the appearance of a small amount of *Cmcm* $LiFePO_4$ alongside a majority olivine phase with the use of $FeC_2O_4{\cdot}2H_2O$ as the iron precursor in an ethylene glycol solvent.[25] In both cases, there were no follow-up studies extending the syntheses to the other three transition metals (M = Mn, Co, and Ni). Recently, our group reported a microwave-assisted solvothermal (MW-ST) synthesis for three distinct polymorphs of $LiCoPO_4$, one of which is the non-olivine *Cmcm* phase.[26] This was achieved with dry tetraethylene glycol (TEG) as the solvent.

Here, we report a facile MW-ST synthesis to easily obtain the *Cmcm* polymorph of all four members of the $LiMPO_4$ family, i.e., with M = Mn, Fe, Co, and Ni. Unlike many previous studies, our synthesis is conducted at low temperatures (<300 °C) and low pressures (<30 bar). The protocol does not require the use of special solvents or preparation of the reaction mixture inside a controlled environment, for example, a glovebox. Readily available metal oxalate precursors and dry TEG solvent play a crucial role in the synthesis. The reducing nature of TEG helped prevent the oxidation of transition-metal ions in oxalate precursors from the +2 to +3 state.[27] Optimization of the reaction conditions leads to high-purity products with correct stoichiometry, with a submicrometer thin platelet-like morphology. *Cmcm* $LiMnPO_4$ is reported for the first time. The metastable nature of the *Cmcm* structure is confirmed, as shown by its irreversible conversion to the olivine structure upon heat treatment at higher temperatures.

EXPERIMENTAL SECTION

Synthesis. The non-olivine (space group *Cmcm*) polymorph of all four members of the $LiMPO_4$ series (M = Mn, Fe, Co, and Ni) was created with the MW-ST process. The reactions took place in 12 mL of tetraethylene glycol (Sigma-Aldrich, 99%), which acted as the reaction medium. To remove any water absorbed by the TEG, it was first dried with 3 Å molecular sieves for 8 h just before starting the syntheses. In all cases, the precursors for lithium and phosphorus were lithium hydroxide monohydrate (Alfa Aesar, 98%) and hydrated liquid phosphoric acid (Fisher Scientific, 85%), respectively. The transition-metal ion precursors for M = Mn, Fe, and Co were metal(II) oxalate dihydrate ($MC_2O_4{\cdot}2H_2O$, Alfa Aesar, 99%) powders. The only exception was $LiNiPO_4$, which was obtained when nickel acetate tetrahydrate (Arcos Organics, 99+%) was used as the nickel source. Before their use, it was very important to crush all the solid precursors into fine powders in an agate mortar with a pestle.

Each reaction took place in a 30 mL borosilicate glass reaction vessel (Anton Paar), which was first filled with 6 mL of TEG. Then, the finely crushed lithium and metal ion precursors were added, which was immediately followed by the dropwise addition of phosphoric acid, before any stirring. The simultaneous mixing of all precursors was vital for avoiding the formation of the olivine phase as an impurity. Several reactions were attempted with varying ratios and concentrations of the precursors. The best results, i.e., correct stoichiometry with minimal impurities, were obtained with the following precise amounts: for $LiMnPO_4$, 100 mg (2.38 mmol) of $LiOH{\cdot}H_2O$, 426.6 mg (2.38 mmol) of $MnC_2O_4{\cdot}2H_2O$, and 163.1 μL (2.38 mmol) of H_3PO_4; for $LiFePO_4$, 75 mg (1.79 mmol) of $LiOH{\cdot}H_2O$, 321.5 mg (1.79 mmol) of $FeC_2O_4{\cdot}2H_2O$, and 122.3 μL (1.79 mmol) of H_3PO_4; for $LiCoPO_4$, 100 mg (2.38 mmol) of $LiOH{\cdot}H_2O$, 436.1 mg (2.38 mmol) of $CoC_2O_4{\cdot}2H_2O$, and 163.1 μL (2.38 mmol) of H_3PO_4; and for $LiNiPO_4$, 50 mg (1.19 mmol) of $LiOH{\cdot}H_2O$, 296.5 mg (1.19 mmol) of $Ni(CH_3CO_2)_2{\cdot}4H_2O$, and 163.1 μL (2.38 mmol) of H_3PO_4. After the addition of all reactants, the mixture was stirred with a magnetic stir bar for ∼1 h and then the remaining 6 mL of TEG was added. A homogeneously dispersed suspension was thus obtained as a result of continued stirring of the reaction mixture for an additional hour. Then, the reaction vessels were tightly sealed with polytetrafluoroethylene (PTFE) lined silicone septa (Anton Paar) and placed in a microwave reactor (Anton Paar Monowave 300) for heating.

The heating procedure consisted of a 5 min preliminary mixing step at 70 °C followed by a rapid heating step at the maximal instrument power of 850 W. This led to a temperature rise at a rate of approximately 100 °C min^{-1} until a desired reaction temperature, as measured by an infrared temperature sensor, was achieved. The reaction mixture was maintained at this temperature for a few minutes before being rapidly cooled to room temperature. The best results were obtained with a hold time of 40 min at 275 °C for $LiMnPO_4$, 10 min at 280 °C for $LiFePO_4$, and 30 min at 300 °C for both $LiCoPO_4$ and $LiNiPO_4$. Throughout the heating procedure in the microwave reactor, the reactants were stirred at 600 rpm with a magnetic stir bar. The peak pressure inside the reaction vessel was always significantly below 30 bar, which is the instrument's limit for safe operation. The precipitated products were separated from the liquid by centrifugation. The products were rinsed three times with acetone to eliminate the remaining solvent. This was accompanied by intermediate ultrasonication treatments lasting 10 min to break up any agglomerates. The rinsed precipitates were dried in an air oven for 2 h at 100 °C to evaporate the acetone while leaving behind a fine powder. The colors of the as-synthesized powders of *Cmcm* $LiMPO_4$ (M = Mn, Fe, Co, and Ni) were pinkish white, gray-green, light pink, and light yellow, respectively. Heat treatments were performed in a carbon-free alumina tube furnace (MTI Corp.) in an ultra-high-purity argon environment. A heating rate between 5 and 10 °C min^{-1} was used, and the desired temperature was maintained for 8 h before cooling.

Characterization. Powder X-ray diffraction (XRD) patterns were recorded on a tabletop diffractometer (Rigaku Miniflex 600) having a Bragg−Brentano geometry. Copper $K\alpha_1$ radiation (λ = 1.5406 Å) was used, and continuous scans were recorded at rates ranging from 1.5 to 4 deg min^{-1}. Preliminary analysis of the powder diffraction patterns was performed with PDXL2 (Rigaku), and Rietveld refinements were conducted with GSAS software. Scanning electron microscope (SEM) images were obtained with a FEI Quanta 650 SEM operating at a voltage ranging from 10 to 20 keV. For enhanced contrast, the samples were sputter coated with gold before being imaged at a magnification of 50000×. Transmission electron microscopy (TEM) and electron diffraction experiments were performed with a JEOL 2010F field emission transmission electron microscope at 200 kV. To determine the elemental composition of the samples, inductively coupled plasma-optical emission spectroscopy (ICP-OES) was performed with a Varian 715-ES spectrometer. The ICP-OES solutions were prepared by first dissolving approximately 4 mg of sample powder in 2−4 mL of aqua regia before diluting with 250 mL of deionized water. Standard solutions (Ricca Chemical Co.) for lithium, phosphorus, manganese, iron, cobalt, and nickel were used to calibrate the ICP-OES instrument. Fourier transform infrared (FTIR) spectroscopy patterns were collected in transmission mode with a Nicolet iS5 instrument. The sample powders were mixed with ultrapure potassium bromide and pressed into transparent thin pallets before the measurements were taken. Differential scanning calorimetry (DSC) was performed

DOI: 10.1021/acs.inorgchem.5b01787
Inorg. Chem. 2015, 54, 10015−10022

with a Netzsch Jupiter STA 449 F3 instrument in an argon environment at a heating/cooling rate of 3.5 °C min^{-1}.

CR 2032 type half-cells were assembled with lithium-metal anodes. The cathodes were comprised of 70 wt % active material, 20 wt % graphitic carbon, and 10 wt % PTFE binder. This cathode mixture was pressed onto a stainless steel mesh and dried in a vacuum oven for 24 h at 150 °C. A commercial electrolyte was used (Novolyte Technologies Purolyte A5 series), which had a 1:1 mixture of ethylene carbonate and dimethyl carbonate with 1 M $LiPF_6$. Cells were assembled in an argon-filled glovebox and tested with a battery cycler (Arbin Instruments).

RESULTS AND DISCUSSION

Morphology and Crystal Structure. As shown in Figure 1, SEM micrographs and low-magnification TEM images of the

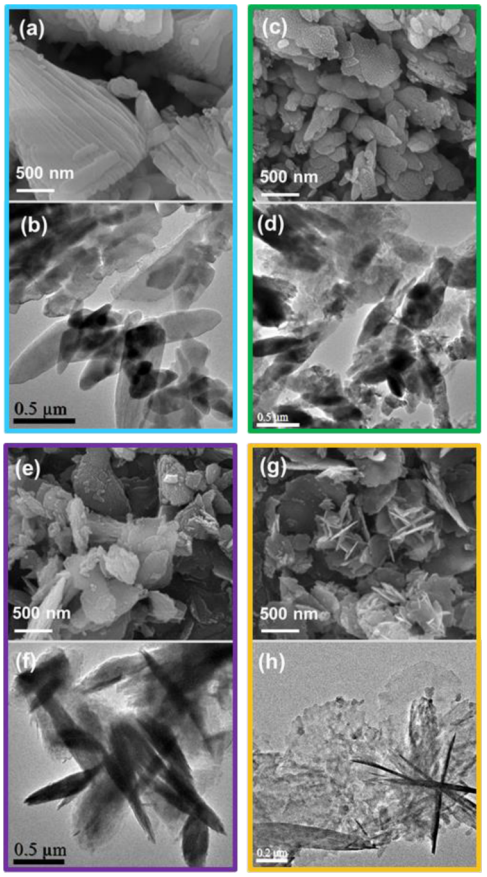

Figure 1. SEM and TEM images showing the submicrometer size thin platelet-like morphology of *Cmcm* $LiMPO_4$ materials: (a and b) M = Mn, (c and d) M = Fe, (e and f) M = Co, and (g and h) M = Ni.

as-synthesized powders reveal a submicrometer thin platelet-like morphology. The thin platelets appear to be stacked on top of each other, most evidently for $LiMnPO_4$. It is also interesting to note that the platelets are especially thin for $LiNiPO_4$. The crystal orientation of the platelets can possibly have a major effect on the properties, based on the atomic arrangement that ends up being on the platelet surface or any ion diffusion pathways along the thin edges.[28]

To identify the orientation of the thin platelets of *Cmcm* $LiFePO_4$, precession electron diffraction was performed with a transmission electron microscope over a large area spanning several particles. Subsequently, an orientation map was generated with an automated crystallographic indexing tool, ASTAR (NanoMEGAS). Figure 2 shows several flat particles having orientations (zone axis) that are indicated primarily by

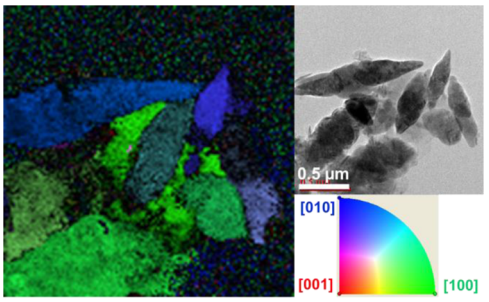

Figure 2. Orientation map and the corresponding TEM image of *Cmcm* $LiFePO_4$ particles. A reference color chart indicates crystallographic directions represented by different colors.

green and blue colors that indicate the [100] and [010] directions, respectively. The nonappearance of red color implies that the corresponding [001] direction lies primarily in the plane of the particles, perpendicular to the zone axis.

To ascertain the novel crystal structure of the $LiMPO_4$ polymorphs, powder XRD patterns were collected. Most studies of $LiMPO_4$ focus on the olivine polymorph, which is represented by the orthorhombic *Pnma* space group. However, for our samples, all XRD peaks could be indexed to the *Cmcm* space group, revealing a different kind of orthorhombic crystal structure. Figure 3 shows the collected XRD patterns as well as the simulated XRD patterns where the fitting has been

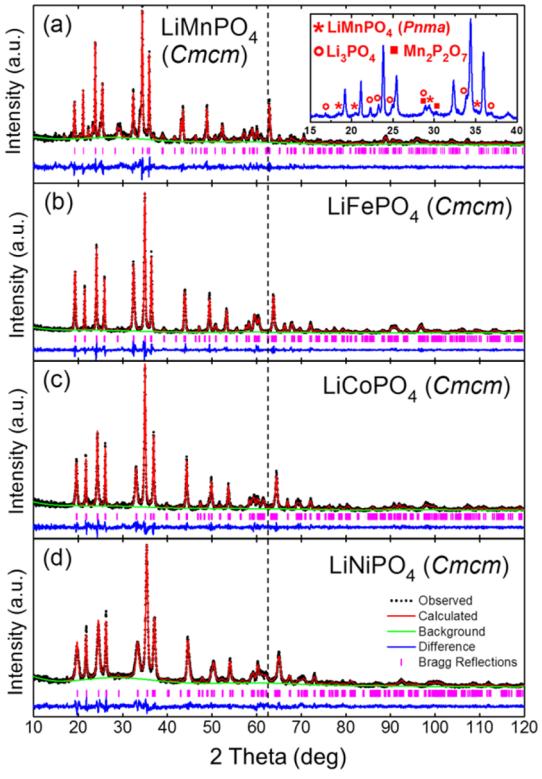

Figure 3. XRD patterns of the as-synthesized *Cmcm* $LiMPO_4$ polymorphs: (a) $LiMnPO_4$, (b) $LiFePO_4$, (c) $LiCoPO_4$, and (d) $LiNiPO_4$. A magnified pattern in panel a highlights the impurity peaks in $LiMnPO_4$. As a reference, the dashed line marks the (242) reflection of $LiMnPO_4$.

DOI: 10.1021/acs.inorgchem.5b01787
Inorg. Chem. 2015, 54, 10015−10022

performed with the Rietveld method.[29] The fitting was performed from 10° to 120° 2θ with β-$LiFePO_4$ (ICSD No. 01-072-7847) as the starting prototype structure.

The collected data match very well with the simulated patterns as indicated by the relatively low values of R_{wp} and χ^2, which are listed in Table 1. The unit cell parameters for

Table 1. Crystallographic Data of $LiMPO_4$ Polymorphs with Orthorhombic Space Group *Cmcm* (63)

	$LiMnPO_4$	$LiFePO_4$	$LiCoPO_4$	$LiNiPO_4$
a (Å)	5.5312(3)	5.5212(7)	5.4236(4)	5.3700(13)
b (Å)	8.3988(3)	8.2708(11)	8.1662(3)	8.1311(17)
c (Å)	6.3160(4)	6.1898(8)	6.2214(3)	6.1397(13)
V (Å^3)	293.41(2)	282.65(10)	275.54(2)	268.08(17)
R_{wp} (%)	14.3	14.0	13.1	7.47
χ^2	1.62	1.47	1.40	1.67

$LiMPO_4$ (M = Mn, Fe, Co, and Ni) that were extracted after the refinement are also listed in Table 1, and additionally, the atomic positions are listed in Table S1 of the Supporting Information. From Table 1, a very elegant decreasing trend can be observed in the unit cell volume on moving from left to right in the periodic table (from Mn to Ni) because of the decreasing ionic radius of the M^{2+} ions. This can also be seen in the form of a shift of the XRD peaks toward larger angles when going from Mn to Ni. To highlight this in Figure 3, as an example, the (242) peak of $LiMnPO_4$ has been marked with a dashed line.

$LiFePO_4$ and $LiCoPO_4$ were obtained as single-phase products in the absence of any impurities. For $LiNiPO_4$, the XRD peaks were relatively broad, as seen in Figure 3d, indicating a smaller crystallite size that can be confirmed from its SEM and TEM images showing ultrathin nanoplates in panels g and h of Figure 1. Nonetheless, there is only one crystalline phase present in the $LiNiPO_4$ pattern corresponding to the *Cmcm* polymorph, and the low-intensity amorphous hump around 30° can be attributed to the poorly crystallized thin particles. Among the four title compounds, $LiMnPO_4$ was the most difficult to obtain as a pure-phase product, even after several attempts with varying synthesis conditions, such as the reaction temperature, duration, precursor concentrations, and pH. Figure 3a shows the impurity peaks that were present even in the most pure sample. A multiphase Rietveld refinement was performed in this case for correct fitting of the XRD pattern. The estimated weight percentage of $LiMnPO_4$ (*Cmcm*) came out to be 71%, whereas those of impurities Li_3PO_4, $Mn_2P_2O_7$, and $LiMnPO_4$ (*Pnma*) were 19, 7, and 3%, respectively.

Both *Cmcm* and *Pnma* space groups belong to the orthorhombic crystal system and have similar symmetry elements. However, for $LiMPO_4$, there are subtle differences between them, particularly in the atomic arrangement. The *Cmcm* structure has one-dimensional chains of edge-shared MO_6 octahedra running along the [001] direction, as illustrated in Figure 4. In contrast, the olivine structure is known to have corner-shared MO_6 octahedra and one-dimensional chains of edge-shared LiO_6 octahedra in the [010] direction. It is along this [010] direction that the lithium ions diffuse in olivine $LiFePO_4$ in a curved pathway.[30] On the other hand, the *Cmcm* structure does not seem to possess such markedly visible lithium diffusion pathways in Figure 4. In fact, the coordination number of lithium in the *Cmcm* arrangement is reduced to four from six in olivine, and this can possibly impede lithium diffusion. Also, the cell volume of the *Cmcm* polymorphs is

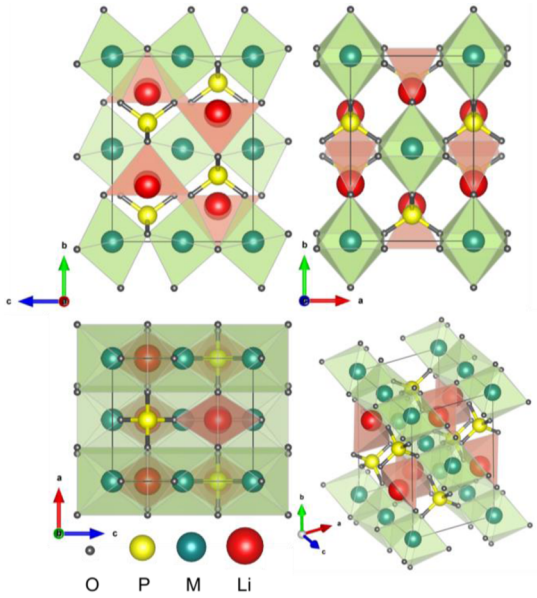

Figure 4. Projections of the *Cmcm* $LiMPO_4$ structure along the three crystallographic axes.

slightly smaller than that of their olivine counterparts, indicating a more snug arrangement of atoms. Additional details about the peculiarities of the two structural arrangements can be found in the literature.[15]

Microwave Synthesis Conditions. Like other glycols, TEG is hygroscopic and absorbs water readily from the atmosphere. We recently demonstrated that the use of fresh, dried TEG is crucial for the formation of the $LiCoPO_4$ *Cmcm* polymorph via the MW-ST method.[26] Even the presence of 2% (v/v) water in the TEG can drastically affect the product's crystal structure. Previously, a similar MW-ST method with TEG as the solvent was shown to produce the olivine polymorphs instead.[31] However, that report did not use dry TEG, which is why the *Cmcm* polymorphs were not formed. Interestingly, in the other two low-temperature papers that reported the pure *Cmcm* $LiFePO_4$ phase, the reactants were either dried on a rotavap or mixed together in a water-free, argon-filled glovebox.[18,24] Therefore, the use of fresh TEG that was dried with molecular sieves in this study was justified.[32] Another important synthesis condition was the use of metal oxalate dihydrate precursors as the transition-metal sources. Unlike soluble metal acetates that were used for our group's previous olivine $LiMPO_4$ MW-ST synthesis,[31] the oxalates that are used in this study do not dissolve much in TEG, which could possibly be promoting the formation of the *Cmcm* polymorph. It is interesting to observe that Ashton et al. obtained *Cmcm* $LiFePO_4$ as a minor phase when using iron oxalate dihydrate with another glycol (ethylene glycol).[25] They asserted that the pressure generated upon evaporation of the water of crystallization from the iron oxalate dihydrate led to this because olivine was being obtained even with dry iron acetate. However, a better explanation could be that their ethylene glycol had some moisture but the use of iron oxalate actually promoted the partial formation of the *Cmcm* phase. Essentially, the use of dry TEG with oxalate precursors distinguishes the method here from previous reports that produced olivine with microwave heating, several of which have been summarized in a 2014 review article.[33]

DOI: 10.1021/acs.inorgchem.5b01787
Inorg. Chem. 2015, 54, 10015−10022

The stoichiometry of the samples was measured with ICP-OES, and the reaction conditions were tweaked to match the $LiMPO_4$ formula within experimental error. With samples deficient in lithium, a particular association is seen between the unit cell parameters and the lithium stoichiometry. For $LiMnPO_4$, it is observed that the (200) and (112) XRD peaks move significantly toward each other when synthesized at a lower reaction temperature (200 °C), as shown in Figure 5a.

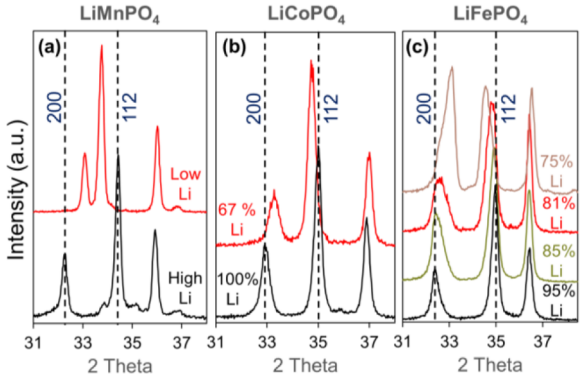

Figure 5. Shifting of the (200) and (112) XRD peaks for lithium deficient *Cmcm* samples indicating a change in the unit cell of (a) $LiMnPO_4$, (b) $LiCoPO_4$, and (c) $LiFePO_4$.

On the basis of the ICP-OES results, it is hypothesized that the low-temperature product is lithium deficient. In Figure 5b, the (200) and (112) peak shifting can also be observed in single-phase *Cmcm* $LiCoPO_4$, which was intentionally synthesized with only 67% lithium precursor and confirmed by ICP-OES. This trend is quite evident for *Cmcm* $LiFePO_4$ as shown in Figure 5c. Before optimization, $LiFePO_4$ had the peaks shifted as well as a lower lithium content, even though the XRD patterns show a single *Cmcm* phase. Interestingly, the measured ICP-OES lithium content gradually increases as the lithium hydroxide precursor was crushed more and more before the reaction, until a nearly perfect stoichiometry was obtained. The lithium content could simultaneously be correlated with the extent of (200) and (112) peak shifting, as seen in Figure 5c.

On the basis of these peak shifts, we conclude that a less than perfect lithium content in the as-synthesized samples is linked with a marked increase in the unit cell parameter *c*, along with a reduction in *a*. Overall, the reaction temperature, reactant concentrations, and precursor crushing are critical for obtaining products with the correct stoichiometry.

Phase Transformation. When the four materials are subjected to a heat treatment in a neutral argon environment, a slow transformation into olivine takes place over a range of temperature, indicating a second-order phase transformation. The materials were heated with 50 °C temperature increments and maintained at the desired temperature for 8 h. The XRD patterns showing the vanishing of *Cmcm* peaks (marked as β) with the simultaneous appearance of the *Pnma* peaks (marked as α) are presented in Figure 6.

For $LiMnPO_4$, the transformation begins as early as 350 °C and ends before 450 °C. It is also interesting to note that when $LiMnPO_4$ was heated, which was prepared at a lower temperature (200 °C) and hence was lithium deficient, the lattice relaxes to a correct stoichiometry structure, marked by the movement of (200) and (112) peaks away from each other, with a simultaneous expulsion of excess Mn and P in the form of a substantial amount of $Mn_2P_2O_7$. Hence, the previously

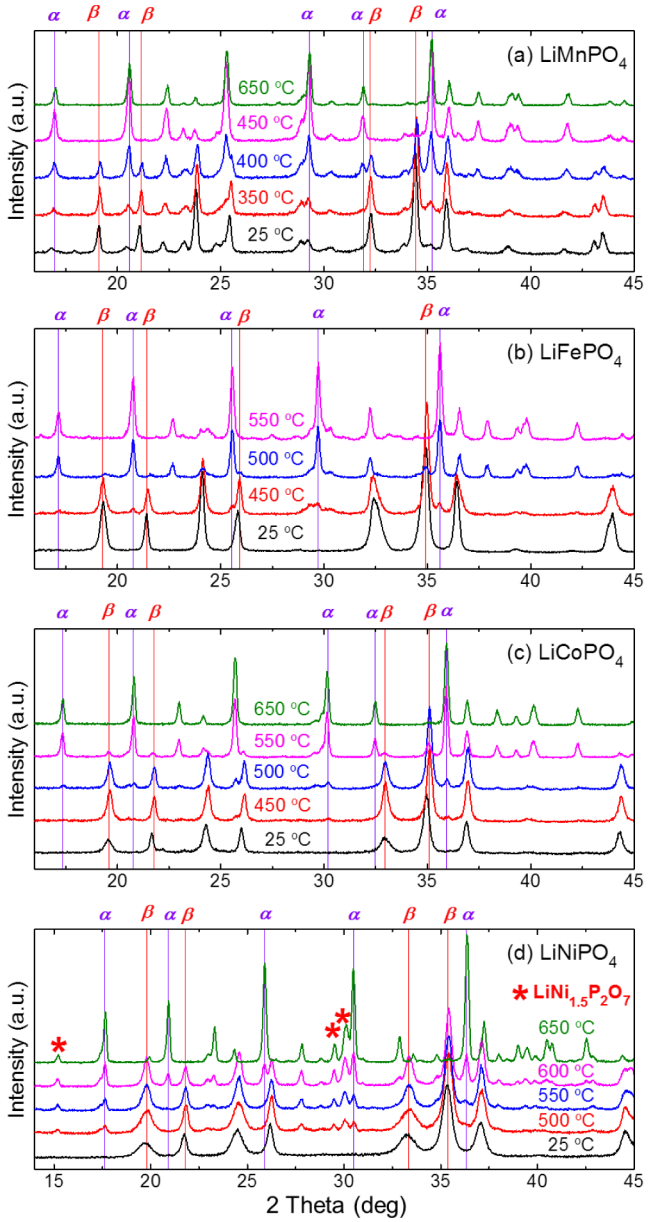

Figure 6. XRD patterns showing the phase transformation of the *Cmcm* (β) polymorph into the *Pnma* (α) structure upon heating in an argon environment for (a) $LiMnPO_4$, (b) $LiFePO_4$, (c) $LiCoPO_4$, and (d) $LiNiPO_4$.

mentioned assertion about the correlation between lithium content and the cell parameters is further strengthened. The *Cmcm* $LiFePO_4$ transforms into olivine between 450 and 550 °C. Fe^{2+} is highly susceptible to oxidation, and even after sufficiently long purging of the tube furnace with argon before heating, a trace amount of the oxidized thin red top layer could be seen after the heat treatment. As shown in Figure 6c, the *Cmcm* $LiCoPO_4$ is transformed at even higher temperatures, between 450 and 600 °C. Among all the $LiMPO_4$ members, $LiNiPO_4$ shows the highest temperature until which the *Cmcm* phase is stable. The olivine phase appears at 500 °C, and the *Cmcm* phase fully disappears only at 650 °C. To quantify the *Cmcm* to olivine phase ratio, multiphase Rietveld refinements were performed. The growth of the olivine phase with an increasing temperature is shown in Figure 7.

DOI: 10.1021/acs.inorgchem.5b01787
Inorg. Chem. 2015, 54, 10015−10022

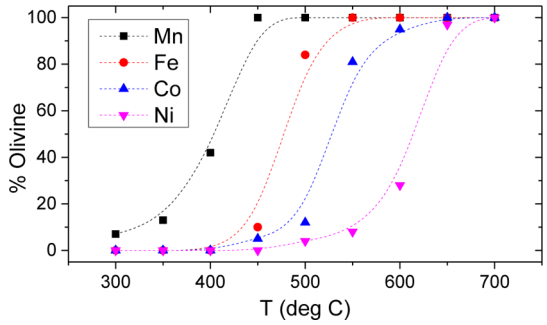

Figure 7. Growth of the olivine phase with increasing temperature during heat treatment of *Cmcm* $LiMPO_4$ (M = Mn, Fe, Co, and Ni).

On the basis of the data presented in Figures 6 and 7, we can conclude that $LiMnPO_4$ undergoes a phase transition from *Cmcm* to olivine at the lowest temperature followed by $LiFePO_4$, $LiCoPO_4$, and $LiNiPO_4$. This trend is possibly due the most compact structure of $LiNiPO_4$, as indicated by the smallest cell volume among all four, which hinders the rearrangement of atoms. The highest thermal stability of *Cmcm* $LiNiPO_4$ could possibly explain its partial appearance in a previous study that involved heating a phosphate-formate precursor at 500 °C.[17] On the other hand, the lowest stability of *Cmcm* $LiMnPO_4$ could also be the reason why it has never been reported in the literature before and why impurity-free synthesis conditions could not be determined in this study.

When DSC was performed on $LiMnPO_4$, a broad exothermic peak could be observed during the heating step in the range of 350−500 °C, as seen in Figure 8. This exothermic event can be

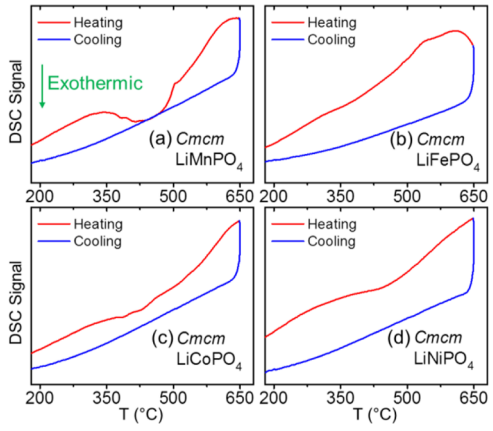

Figure 8. DSC heating and cooling curves of the as-synthesized *Cmcm* $LiMPO_4$ polymorphs: (a) $LiMnPO_4$, (b) $LiFePO_4$, (c) $LiCoPO_4$, and (d) $LiNiPO_4$.

attributed to the phase transformation. However, for the other three materials, such a clearly distinguishable DSC event cannot be conclusively assigned to the phase transformation observed upon heating. For all four *Cmcm* materials, XRD confirmed the conversion into the olivine phase after the DSC experiment. The absence of any peak in the cooling curves indicates the irreversible nature of the phase transformation. DSC further confirms the fact that the *Cmcm* polymorphs are higher-energy metastable phases and a kinetically driven synthesis process like MW-ST is the only way to obtain them. The thin platelet-like morphology is also a unique feature of the MW-ST-synthesized *Cmcm* $LiMPO_4$ polymorphs. This is indicated by a conversion to nanosphere/rod type particles for the olivine materials obtained after heat treatment, as seen in the SEM micrographs in Figure 9.

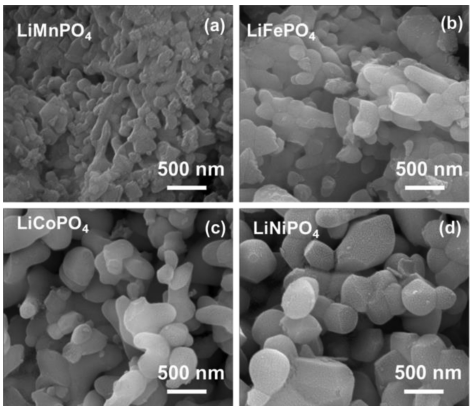

Figure 9. SEM micrographs of the $LiMPO_4$ samples after heat treatment leading to the conversion to olivine for (a) $LiMnPO_4$, (b) $LiFePO_4$, (c) $LiCoPO_4$, and (d) $LiNiPO_4$.

In Figure 10, the FTIR spectra are shown for the *Cmcm* materials as well as their olivine analogues obtained after heat

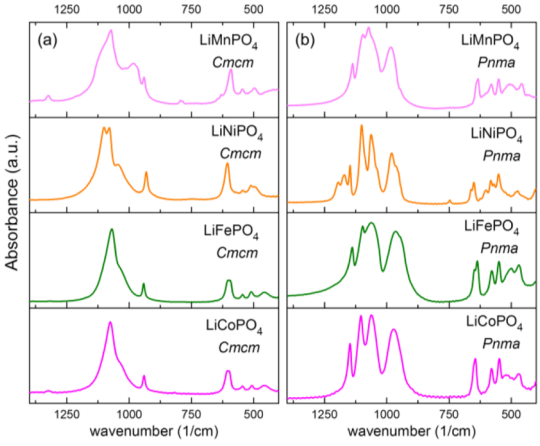

Figure 10. FTIR spectra of (a) the *Cmcm* $LiMPO_4$ materials and (b) their respective *Pnma* olivines obtained after heat treatment.

treatment. The PO_4^{3-} anion group has bond stretching modes as indicated by the absorption peaks from 900 to 1200 cm^{-1}, whereas the bending modes are from 400 to 700 cm^{-1}.[34] The FTIR spectra for the two polymorphs are noticeably different from each other because of the different site symmetry. This indicates that these two polymorphs have different properties even though the space groups are very similar in terms of symmetry.

Electrochemistry. In Figure 11, the cyclic voltammetry (CV) results for the *Cmcm* $LiMPO_4$ materials tested in half-cells as cathodes for lithium ion batteries are presented. The tests were performed at a scan rate of 5 mV s^{-1}. Similar to the CV reports in the literature[18,24] for *Cmcm* $LiFePO_4$, a reversible electrochemical activity at ~3.0 V was observed for our samples, but the charge capacity associated with it is too small for practical application as a lithium ion battery cathode material. *Cmcm* $LiMnPO_4$, $LiCoPO_4$, and $LiNiPO_4$ show only a charging peak at 4.2, 4.2, and 4.3 V, respectively, without any discharge peak. A small discharge peak observed for $LiMnPO_4$

DOI: 10.1021/acs.inorgchem.5b01787
Inorg. Chem. 2015, 54, 10015−10022

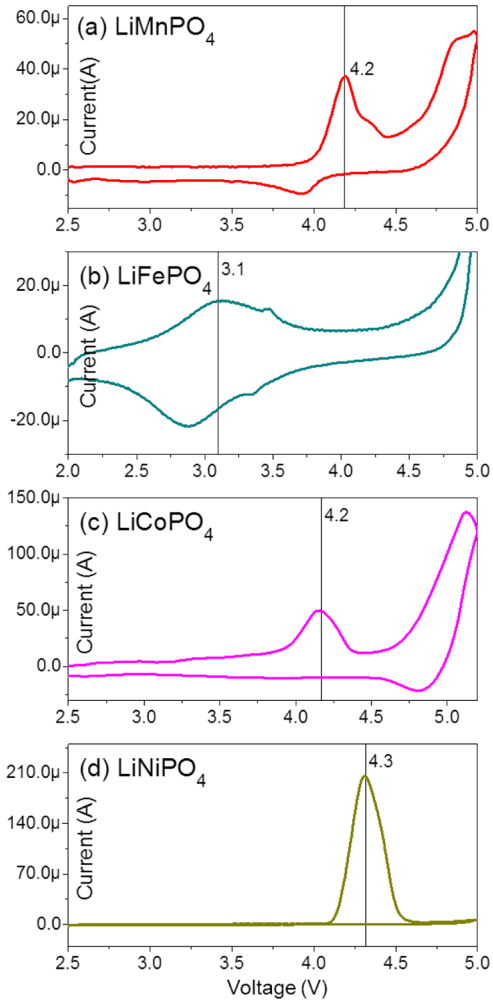

Figure 11. Cyclic voltammograms of *Cmcm* $LiMPO_4$ materials for (a) $LiMnPO_4$, (b) $LiFePO_4$, (c) $LiCoPO_4$, and (d) $LiNiPO_4$.

is probably due to the small amount of olivine impurity in the sample. For M = Co and Ni, the charged coin cells were carefully opened inside a glovebox and XRD was performed on the harvested electrodes. No evidence of peak shifting or structural changes was found, and the XRD pattern matched well with that of the as-synthesized powders. The exact cause of the charging peaks is unknown but could be an irreversible electrolytic side reaction. Overall, the *Cmcm* materials perform poorly as lithium ion battery cathodes.

CONCLUSION

A facile, low-pressure, and low-temperature microwave-assisted solvothermal synthesis with tetraethylene glycol as the solvent has been utilized to obtain the orthorhombic *Cmcm* polymorph of all four members of $LiMPO_4$ (M = Mn, Fe, Co, and Ni). Of these, $LiMnPO_4$ has never been reported before. The *Cmcm* polymorphs have a different crystal structure compared to that of the thoroughly studied olivine polymorphs. Correct selection of the reaction temperature, reaction duration, precursors, and solvent results in near stoichiometric products with minimal impurities, as characterized by XRD and ICP-OES. The metastable nature of the structure is revealed when the *Cmcm* phase transforms into the more stable olivine phase upon being heated with a sluggish and irreversible phase transition. Even though the electrochemistry of the *Cmcm* polymorphs is not favorable as lithium ion cathodes, the comprehensive facile synthesis has opened up the possibility of studying these polymorphs for fundamental understanding.

ASSOCIATED CONTENT

Supporting Information

The Supporting Information is available free of charge on the ACS Publications website at DOI: 10.1021/acs.inorgchem.5b01787.

Atomic positions for the *Cmcm* $LiMPO_4$ polymorphs obtained after Rietveld refinement (PDF)

AUTHOR INFORMATION

Corresponding Author

*E-mail: manth@austin.utexas.edu.

Notes

The authors declare no competing financial interest.

ACKNOWLEDGMENTS

This work was supported by the office of Vehicle Technologies of the U.S. Department of Energy under Contract DEAC0205CH11231 (BATT Program). We thank Dr. Yubao Zhao and Dr. Karalee Jarvis for helping with the TEM experiments and analysis.

ABBREVIATIONS

MW-ST, microwave-assisted solvothermal; TEG, tetraethylene glycol; XRD, X-ray diffraction; SEM, scanning electron microscope; ICP-OES, inductively coupled plasma-optical emission spectroscopy; FTIR, Fourier transform infrared; PTFE, polytetrafluoroethylene; TEM, transmission electron microscopy; DSC, differential scanning calorimetry; CV, cyclic voltammetry

REFERENCES

(1) Masquelier, C.; Croguennec, L. *Chem. Rev.* **2013**, *113*, 6552−6591.
(2) Manthiram, A.; Goodenough, J. B. *J. Power Sources* **1989**, *26*, 403−408.
(3) Manthiram, A.; Goodenough, J. B. *J. Solid State Chem.* **1987**, *71*, 349−360.
(4) Padhi, A. K.; Nanjundaswamy, K. S.; Goodenough, J. B. *J. Electrochem. Soc.* **1997**, *144*, 1188−1194.
(5) Yuan, L. X.; Wang, Z. H.; Zhang, W. X.; Hu, X. L.; Chen, J. T.; Huang, Y. H.; Goodenough, J. B. *Energy Environ. Sci.* **2011**, *4*, 269−284.
(6) Aravindan, V.; Gnanaraj, J.; Lee, Y. S.; Madhavi, S. *J. Mater. Chem. A* **2013**, *1*, 3518−3539.
(7) Hu, M.; Pang, X.; Zhou, Z. *J. Power Sources* **2013**, *237*, 229−242.
(8) Wolfenstine, J.; Allen, J. *J. Power Sources* **2005**, *142*, 389−390.
(9) Zaghib, K.; Guerfi, A.; Hovington, P.; Vijh, A.; Trudeau, M.; Mauger, A.; Goodenough, J. B.; Julien, C. M. *J. Power Sources* **2013**, *232*, 357−369.
(10) Wang, J.; Sun, X. *Energy Environ. Sci.* **2012**, *5*, 5163−5185.
(11) Huang, Y. H.; Goodenough, J. B. *Chem. Mater.* **2008**, *20*, 7237−7241.
(12) Hong, J.; Wang, F.; Wang, X.; Graetz, J. *J. Power Sources* **2011**, *196*, 3659−3663.
(13) Akimoto, S.; Taniguchi, I. *J. Power Sources* **2013**, *242*, 627−630.
(14) Harrison, K. L.; Bridges, C. A.; Paranthaman, M. P.; Segre, C. U.; Katsoudas, J.; Maroni, V. A.; Idrobo, J. C.; Goodenough, J. B.; Manthiram, A. *Chem. Mater.* **2013**, *25*, 768−781.

DOI: 10.1021/acs.inorgchem.5b01787
Inorg. Chem. 2015, 54, 10015−10022

(15) García-Moreno, O.; Alvarez-Vega, M.; Garcia-Alvarado, F.; Garcia-Jaca, J.; Gallardo-Amores, J. M.; Sanjuan, M. L.; Amador, U. *Chem. Mater.* **2001**, *13*, 1570−1576.
(16) Amador, U.; Gallardo-Amores, J. M.; Heymann, G.; Huppertz, H.; Moran, E.; Arroyo y de Dompablo, M. E. *Solid State Sci.* **2009**, *11*, 343−348.
(17) Koleva, V.; Stoyanova, R.; Zhecheva, E. *Eur. J. Inorg. Chem.* **2010**, *2010*, 127−131.
(18) Voß, B.; Nordmann, J.; Kockmann, A.; Piezonka, J.; Haase, M.; Taffa, D. H.; Walder, L. *Chem. Mater.* **2012**, *24*, 633−635.
(19) Bilecka, I.; Niederberger, M. *Nanoscale* **2010**, *2*, 1358−1374.
(20) Baghbanzadeh, M.; Carbone, L.; Cozzoli, P. L.; Kappe, C. O. *Angew. Chem., Int. Ed.* **2011**, *50*, 11312−11359.
(21) Zhu, Y. J.; Chen, F. *Chem. Rev.* **2014**, *114*, 6462−6555.
(22) Harrison, K. L.; Manthiram, A. *Chem. Mater.* **2013**, *25*, 1751−1760.
(23) Jähne, C.; Neef, C.; Koo, C.; Meyer, H. P.; Klingeler, R. *J. Mater. Chem. A* **2013**, *1*, 2856−2862.
(24) Zeng, G.; Caputo, R.; Carriazo, D.; Luo, L.; Niederberger, M. *Chem. Mater.* **2013**, *25*, 3399−3407.
(25) Ashton, T. E.; Laveda, J. V.; MacLaren, D. A.; Baker, P. J.; Porch, A.; Jones, M. O.; Corr, S. A. *J. Mater. Chem. A* **2014**, *2*, 6238−6245.
(26) Kreder, K. J., III; Assat, G.; Manthiram, A. *Chem. Mater.* **2015**, *27*, 5543−5549.
(27) Moorhead-Rosenberg, Z.; Harrison, K. L.; Turner, T.; Manthiram, A. *Inorg. Chem.* **2013**, *52*, 13087−13093.
(28) Zhao, Y.; Peng, L.; Liu, B.; Yu, G. *Nano Lett.* **2014**, *14*, 2849−2853.
(29) Rietveld, H. M. *J. Appl. Crystallogr.* **1969**, *2*, 65−71.
(30) Nishimura, S.; Kobayashi, G.; Ohoyama, K.; Kanno, R.; Yashima, M.; Yamada, A. *Nat. Mater.* **2008**, *7*, 707−711.
(31) Murugan, A. V.; Muraliganth, T.; Ferreira, P. J.; Manthiram, A. *Inorg. Chem.* **2009**, *48*, 946−952.
(32) Williams, D. B. G.; Lawton, M. *J. Org. Chem.* **2010**, *75*, 8351−8354.
(33) Yu, F.; Zhang, L.; Zhu, M.; An, Y.; Xia, L.; Wang, X.; Dai, B. *Nano Energy* **2014**, *3*, 64−79.
(34) Nakamoto, K. *Infrared and Raman Spectra of Inorganic and Coordination Compounds*, 6th ed.; Wiley: New York, 2008.

DOI: 10.1021/acs.inorgchem.5b01787
Inorg. Chem. 2015, 54, 10015−10022